

Research paper ■

Segmentation Methods in Atherosclerosis Vascular Imaging

Rakesh Sharma, Avdhesh Sharma

Abstract. Vascular stenosis measurement evaluates the cardiovascular risk and vascular disease by use of 3D segmentation. 3D segmentation methods of vascular MRI images are used in vascular feature characterization by parametric deformable models, feature contour map and contrast enhancement methods. Segmentation is done by object delineation and recognition using surrogate vascular marker. T1 weighted and T2-weighted segmentation methods use parametric color-coded feature maps and 3D reconstruction rendered images to display different plaque and vascular wall features. Segmented wall thickness, lumen area and plaque constituents appear significant cardiovascular risk indicators after automated segmentation of vascular features.

■ **Infor Med Slov:** 2006; 11(2): 52-69

Authors' institutions: Department of Medicine, Baylor College of Medicine, Houston, TX, USA (RS), Postgraduate Department of Biochemistry, North Maharashtra University, Jalgaon, Maharashtra, India (RS), Department of Electrical Engineering, Indian Institute of Technology, New Delhi, Delhi, India (AS), Department of Electrical Engineering, Jay Narain Vyas University, Jodhpur, Rajasthan, India (AS).

Contact person: Rakesh Sharma, 901 West Jefferson Street, Jeffwood B-7, Tallahassee, FL 32304, USA. email: rs2010@columbia.edu.

Introduction

Atheromatous plaques develop in the walls of large and medium arteries. These include thoracic and abdominal arteries, carotid and coronary arteries. Common carotid artery bifurcates into two internal and external branches. Progressive enlargement of plaques narrows the arterial lumen, causing vascular stenosis and occlusion.

Atherosclerosis may become acute asymptomatic when an unstable atheromatous plaque ruptures. The contents of ruptured plaque are highly thrombogenic, causing arterial occlusion 'emboli' and lead to the development of aneurysm. These cause tears longitudinally in the arterial wall. Ultimately these tears in wall allow blood to escape from their vessel lumen. Vascular magnetic resonance imaging (MRI) imaging helps to define the nature and extent of vascular disease and therapy monitoring for progression or reoccurrence after therapy. Image processing is used to extract information from vascular imaging. Carotid artery segmentation locates the incidence of atheroma formation near to bifurcation region. AHA classification distinguished the plaque MRI features and scored criteria of atherosclerosis disease burden.¹ Glagov et al.² classified and defined morphological segments of common carotid (C1 C2), bifurcation (B1 B2), external and internal branches (E1, I1). Atherosclerosis in vivo evaluation mainly depends on accurate carotid segmentation for vessel wall, plaque chemical composition and lumen measurement. However, many controversial questions in vascular imaging are important such as: isolated plaque or multiple lesions, % occlusion or narrowing of lumen in vascular segment, site of occlusion either distal or proximal to the lesion, presence of collateral vessels to provide blood flow around lesion, abnormal blood flow patterns.

In the present paper, locally developed 3D segmentation method is demonstrated based on algorithms of object delineation and object recognition of atherosclerosis vascular wall and plaque features; surrogate markers; validation with experimental phantom; finally theory of

evaluation of segmentation method. Our focus was to demonstrate the power of segmentation to visualize carotid vascular MRI features and plaque constituents as possible cardiovascular risk predictors. This segmentation approach may be applied to other vessels and arteries such as femoral and renal arteries.

Vascular Image Segmentation

Classifiers and segmentation algorithms extract out features and characteristics of image primitives or *a priori* information. This *a priori* information is boundary-based and region-based edge-detection approximate gray-level values of carotid vessel wall tissue, spatial location of bifurcation to initialize a threshold-based or spatial transformation or boundary detection and interpretation of wall layers. Segmentation depends on thresholding that suffers from noise and sampling artifacts. Deformable models minimize these problems in segmentation. Deformable models are 'curves' or 'surfaces' defined within image domain that can move under the influence of internal forces within the curve or surface it self and external forces that are computed from the image data.

Deformable models as SNAKES or active contours

Parametric deformable models use 'snakes' and 'curves'. Snakes show direct interaction with the model and lead to fast-real time implementation. These 'snakes' are also known with other names such as balloons, surfaces etc. Deformable models may be geometric models. Parametric deformable models may be two types: 'energy minimizing formulation' and a 'dynamic force formulation'.

Energy Minimization Formulation

It finds a parameterized curve with minimum internal energy (tension or the smoothness of contour) and potential energy (local minima at the image intensity edges occurring at object boundaries). 'Curve' may be defined as

$X(s) = (X(s), Y(s))$, $s \in [0,1]$ which moves through the spatial domain of an vascular image to minimize the following energy functional component:

$$E(X) = S(X) + P(X) \quad (1)$$

where $E(X)$, $S(X)$ and $P(X)$ are energy functional components of curve.

Dynamic Force Formulation

The force formulation represents the external force as dynamic formulation by dynamics of a contour $X(s,t)$:

$$\mu d^2X/dt^2 = F_{damp}(X) + F_{in}(X) + F_{ext}(X) \quad (2)$$

where $\mu=0$ (in segmentation) is coefficient that has mass unit and F_{damp} is the damping (or viscous) force defined as $-\gamma dX/dt$ with γ being the damping coefficient. Several external forces are now applicable to deformable contours and surfaces such as multiscale Gaussian potential force, pressure force, distance potential force, Gradient vector flow, dynamic distance force, interactive force. Deformable models generate 'contours' by finite difference method, dynamic programming, greedy algorithm, marching algorithm.³

Interpretation of Features from Segmentation

Color-coded feature classification aims to the specific identification of plaque components. Descriptions of regions may be either "Contour-based" or "Region-based" (in terms of effective diameter, circularity and projection).⁴

Classification vs. Representation

Color-coded feature based classification of plaque tissue represents the compositional and dimensional properties of atherosclerosis lesions. However, question of diffuse or semi-solid, fibrous, collagenous or elastic, still remains a problem into one of a finite number of mutually exclusive

classes. A 'classifier' needs to designate and separate points representing distinct 'classes' with assumption that matching points tend to be closer with each other away from other points. The subset of features yielding minimum $P(e)$ represents best set and parametric classifier (Bayes method) uses probability structure data class-by-class to generate 'feature set' or class decision for a given sample. If data is insufficient, non-parametric classifier methods (ANN, KNN) are used.⁵

Quantitative Analysis of Segmented Images and Algorithms

The segmentation goals are identification of accurate vessel morphology, topology (angles and curvatures), correct plaque labeling and voluming. It is accomplished by measurement of wall thickness, lumen and plaque size. Automatic segmentation requires robust and quick methods to perform accurate separation and identification of vascular structure with minimal amount of user interaction. This allows the selective visualization (region of interest display), and quantitation of vascular function.

A priori Knowledge Based Image Segmentation

It depends on *a priori* knowledge. It may involve knowledge of approximate gray-level value of a tissue class to initialize a threshold based method, spatial location of tissue or organs for automated selection of training points for a classifier, or shape of object. Training points design the spatial transformations and constraints for the boundary detection algorithms.⁶ This information can be used to improve the specificity and sensitivity of the low-level segmentation algorithms.

Vasculature Assessment (Object Extraction) Algorithm

Extraction of bifurcation segment starts from operator-choice of seed point using following strategy. The segment is a 3D portion of vasculature. Using seed point, image intensity ridges are extracted out approximately same vessel dimensions utilizing *a priori* information supplied. The vessel dimensions can be measured proportional to the scale.⁶ The steps are:

1. Geometry-based semi-automatic segmentation using carotid artery magnetic resonance angiography (MRA) volume to extract bifurcation segment in the region of interest;
2. Comparison of extracted vessel segments with maximum intensity projection of MRI data in the region of interest. If bifurcation segment is missing, repeat step 1;
3. Iterative construction of carotid artery bifurcation segment;
4. 3D visualization and interactive editing of resulting bifurcation artery segment.

Artery Visualization and Suppression of Overlapping Veins

Vessel segmentation uses automated process after operator selects two points (start and end points) of vessel. At the start point location, a search for the vessel borders is performed by dynamic programming in a plane perpendicular to the vessel segment (two interactively marked points). Dynamic programming identifies approximately elliptic border of artery cross-section and a centroid of vessel region is calculated as new centerline point. It is mapped to the next plane of vessel segment in the direction of segment end.⁷ The steps are:

1. Maximum intensity projection of bifurcation region of interest in 3D

2. Interactive identification of start and end points of adjacent veins, and their removal;
3. Interactive generation of targeted MIP image
4. Bifurcation segment labeling
5. Repetition of steps 2, 3, 4 until resulted bifurcation MIP image.

SNAKES Algorithm

'Snakes' are deformable active contour models attracted to image features such as edge, lines, contours etc. Snake is a energy-minimizing spline guided by internal constraint forces and influenced by external forces that pull it towards image features. These snakes pass by edges. It behaves as balloon and skips high intensity points and passes over edges that are weaker intensity points. The starting point for SNAKES algorithm is manually chosen as a single seed point at common carotid artery (centroid). Further, application of 3×3 Sobel edge detector mask to carotid MRA images enhances the speed of snake energy minimization. At optimized settings of edge force, expansion force and use of constants, several node points approximate a contour. The vertices of the obtained contours are placed in areas with significant values of the image gradients. The algorithm is the equation determining vertex movement. Equation (3) defines the new iterative process for finding the SNAKE location. A contour by a set of points $v(s) = (x(s), y(s))$ on an image parameterized with respect to the contour arc length s . The total energy of the active contour is the integration of local energies along its normalized contour, which is written as

$$E_{\text{snake}} = \int_{0..1} E_{\text{int}} + E_{\text{ext}} ds \quad (3)$$

E_{int} represents the internal energy of the snake that measures the continuity and smoothness of the contour. The internal energy can be defined as $E_{\text{int}} = a(s) |v_s(s)|^2 + b(s) |v_{ss}(s)|^2$, where v_s and v_{ss} are the first and second derivative of v by the arc length s . E_{ext} are external forces, which can be

lines, edges and terminations derived from the image.

$$\begin{aligned} E_{\text{ext}}(v) &= - \int_{\Omega} g_o (|f_M * I| + A * I) ds \\ &= - \int_{\Omega} F(v) ds \end{aligned} \quad (4)$$

where f_M represents the Macleod operator, I denotes the raw image, g_o is the gravity constant, A is a positive weighting factor, and $*$ represents the convolution operator. In addition, Ω defines a local area in which the gravity is assumed to be effective to current position v . Depending on positive or negative value of f_M the contour vertices move forward or backward along their normal vectors n . Function f in Equation (4) looks along the vector n for the maximum value of dot product between image gradient and vector n . The neighborhood of radius b (in one dimensional space) maxima point can be searched. The search step is set to a fractional part of a pixel. The gradient computed value gives an intensity difference on a similar distance. The image intensity is calculated by means of bilinear interpolation. If the maximum gradient is found on the outer side of the contour, function f obtains a positive value and the vertex moves towards the maxima point is searched. At maxima point inside the contour, the vertex moves in the opposite direction. The algorithm enables the user to change the radius b as one of the parameters control the distance of the contour edge located in the expected location. In this algorithm, snake vertices oscillate near the sharpest edge based on the assumption that the initial contour for locating the intima always lies above the sub-intima region. So the iterative process must be stopped after a certain number of iterations (usually ten iterations). If the function f_M is set to zero in Equation (4) the algorithm can be used for contour smoothing by using the sequence of ten iterations of the full snake algorithm, five iterations of smoothing and again five iterations of the snake algorithm. The smoothing phase avoids spurious edge for the smooth curved object shape.

Tracking the Carotid Aorta

This method produces surface as a set of voxels with user's supervision during segmentation process and parameter correction.⁸ The algorithm steps are described in the procedure for aorta tracking based on connectivity:

1. Initialization in one of the slices (just under the aortic arch) and automatically finding starting point and performs segmentation for other slices;
2. Find the descending aorta in all slices under the initial one;
3. The initial point in the next slice is determined as an average position of all snake points in the previous slice;
4. The parameter associated with pixel intensity is corrected for each slice, so that the product p and av is constant, where p is the balloon parameter, av is an average pixel value computed for certain neighborhood of the initial point; and
5. Segmentation must be repeated only for the skipped slices. A maximum number of iterations is done that is acceptable for a contour approximation.

If the contour exceeds this number, its average position is not used as an initial point for the next slice. In that case the last regular snake is used to compute the initial point. This feature is used to track the aorta, in cases when a single image can destroy an entire set by moving the initial point completely out of the desired area of the aorta.

Dynamic Programming Algorithm

It computes the optimal paths in a graph for searching boundaries in one direction based on the principle that "an optimal policy has the property of whatever the initial state and initial decision are, the remaining must constitute an optimal policy with regards to the state resulting from the

first decision".⁹ So, the choice of a transition from n_j to n_{j+1} can be based on only the cost of optimal path to n_j and the local cost associated with a move from n_j to n_{j+1} .

Both border detection searches are performed in small bands along the approximate border positions in full resolution data.

Plaque contrast enhancement methods

In vivo MRI imaging evaluation of 1-mm thick carotid artery image slice with plane resolution of 0.1 mm visualizes atheroma tissue components appearing as dark, brighter and gray areas. Carotid artery wall mainly consists outer layer intima, outlined by epithelium collagen embedding media which is the seat of connective tissue components like elastin, collagen, fibrous muscles, blood capillaries and deposits including thrombus, plaque etc.

Two important plaque components are atheromatous core and fibrous cap generate contrast by selecting different TE and TR values.¹⁰ Apparently the major presence of water hydrogen atoms in the core in comparison with lipids allows better NMR signal by frequency selective methods. T2 weighted sequences using broad range of TE and TR provide good contrast between plaque components with lesser effect of noise, motion artifacts, acquisition time demand and longer TE.

Segmentation and evaluation

Evaluation of segmentation method

Evaluation is done by 'object recognition' and 'delineation' that depend upon contrast-to-noise ratio in segmentation. Image (gray level) display, interpolation, filtering, and registration operations depend on image segmentation process.

Quantitative evaluation of segmentation algorithms, at the outset, specifies the quality of

segmentation in terms of technique stability and its accuracy depending on various factors:

- A: An application or task; example: volume estimation of atherosclerosis plaque or scene.
- B: A body region; example: carotid artery bifurcation.
- C: An imaging protocol; example: FSE MR imaging with a particular set of parameters. Scene: A 3D volume image, denoted by $\xi = \{C, f(c)\}$, where C is a rectangular array of voxels, and $f(c)$ denotes the scene intensity of any voxel c in C. ξ may be a vectorial scene, meaning that $f(c)$ may be a vector whose components represent several imaged properties. C is referred to as abinary scene if the range of $f(c)$ is (0, 1).
- T: A set of slice-by-slice scenes acquired for the given application domain $\langle X, Y, Z \rangle$.

Segmentation of an object 'o' in a given scene acquired for an application domain $\langle X, Y, Z \rangle$ is the process of defining the region/ boundary of 'o' in the given scene. It consists of two related tasks - recognition and delineation. Recognition is a high-level and qualitative task of determining roughly the whereabouts of the object in the scene. Delineation is a lower-level and quantitative task of specifying the precise location and extent of object's region/boundary in the scene.

Suppose the output of any segmentation algorithm corresponding to a given scene $e = (C, f)$ is a set of voxels $O \subset C$. This set represents the region occupied by (the support of) an object o of B in C. The fuzzy object defined by o in e is a scene $e_o = (C, f_o)$, where, for any $c \in C$,

$$f_o(c) = \begin{cases} \eta(f(c)), & \text{if } c \in O; \\ 0, & \text{otherwise.} \end{cases} \quad (5)$$

Suppose, e_o is itself a fuzzy object. Here η is a function that assigns a degree of objectiveness to every voxel c in O depending on the scene intensity $f(c)$. Segmentation in C represents object

o in B by O and the corresponding fuzzy object by e_o .

The *efficacy* of vascular segmentation method M in an application domain $\langle X, Y, Z \rangle$ depends on three factors: *precision* which represents repeatability of segmentation taking into account all subjective actions required in producing the result; *accuracy*, which denotes the degree to which the segmentation agrees with truth; *efficiency*, which describes the practical viability of the segmentation method.

For carotid vessel as fuzzy object, let us assume the operations as: $e_{ox} = (C, f_x)$, $e_{oy} = (C, f_y)$ and $e_{oz} = (C, f_z)$ be any fuzzy objects defined by the same object o in a scene e . Then, the *cardinality* of the fuzzy object is defined as $|e_{ox}| = \sum_{c \in C} f_x(c)$. Fuzzy set union $e_{oz} = e_{ox} \cup e_{oy}$ is defined for any $c \in C$ by $f_z(c) = \max(f_x(c), f_y(c))$. Fuzzy set intersection $e_{oz} = e_{ox} \cap e_{oy}$ is defined for any $c \in C$ by $f_z(c) = \min(f_x(c), f_y(c))$.

Fuzzy set difference $e_{oz} = e_{ox} - e_{oy}$ is defined for any $c \in C$ by

$$f_z(c) = \begin{cases} f_x(c) - f_y(c), & \text{if } f_y(c) \geq 0; \\ 0, & \text{otherwise.} \end{cases} \quad (6)$$

A fuzzy masking operation, $e_{oz} = e_{ox} \bullet e_{oy}$ called 'inside', is defined for any $c \in C$ by

$$f_z(c) = \begin{cases} f_x(c), & \text{if } f_y(c) \neq 0; \\ 0, & \text{otherwise.} \end{cases} \quad (7)$$

Another fuzzy masking operation is $e_{oz} = e_{ox} \circ e_{oy}$, called 'outside'. It is defined for any $c \in C$ by

$$f_z(c) = \begin{cases} f_x(c), & \text{if } f_y(c) = 0; \\ 0, & \text{otherwise.} \end{cases} \quad (8)$$

Surrogate of Truth

In case of in vivo MRI patient images, it is almost impossible to establish absolute true segmentation; some surrogate of truth for comparison is needed. Our basic objective was to develop this framework in the light of assumption that operator manually

outperform computer algorithms in recognition tasks, while automated computer algorithms are far more efficacious in delineation than it is done manually. Accordingly, the surrogates that were used reflected this objective. However, the delineation and recognition aspects are two separate methods.

Object Delineation

Five possible choices of the vascular surrogate of truth for delineation are outlined below.

Manual Delineation: It is easier but it is not exact. Suppose, corresponding to a given set T of scenes for the application domain $\langle X, Y, Z \rangle$, manual delineation in either of these forms produces a set T_{td} of scenes representing the fuzzy objects defined by the same object represented in the scenes in T . Manual 'delineation' produces a hard set o for each scene $C \in T$, which is later converted to a fuzzy object. There are several ways of averaging the results to get binary scenes, T_{td} . The binary objects (o) segmented in each scene $C \in T$ in multiple trials may be averaged first and then the fuzzy object may be computed.

Automated delineation: Automated delineation of vessel boundaries and edge identification assesses carotid artery stenosis. An example of automated contour delineation of vascular boundaries and measurement of wall thickness by using SNAKE algorithm is demonstrated in present report. In this approach, transform pixel coordinates of SNAKE boundary from x, y to radial r, θ are used to delineate the outer and inner boundaries of the vessel to measure wall thickness.

Simulated Scenes - 3D Deformations: 3D deformations generate simulated scenes to capture variations for segmentation. The same method was applied for manual segmentation. The complete set of scenes (original + deformed) in this case constitutes T , and the complete set of segmentations represents T_{td} .

Simulated Scenes - Cutoff Regions: Another method to simulate vascular scenes first creates an

ensemble of “cut-outs” of object regions from actual acquired scenes. In second step, these “cutouts” of object regions get buried realistically in different scenes. Each cut-out may be segmented by appropriate segmentation method viz. validated, seed growth, supervised etc. The cut-out regions contain the object region with a background tissue region only without any other confounding tissue regions the resulting scenes and the segmentations constitute T and T_{id} , respectively.

Contour Delineation: Our semi-automatic contour delineation technique was modification of method Ladak et al.¹¹ based upon the discrete dynamic contour (DDC). A DDC is a polyline, a sequence of points connected by straight-line segments that deforms to fit features in an image. DDC drives outwards through a balance of image-derived forces (which define the edges of the vessel), internal forces (which keep the DDC smooth in the presence of noise), and damping forces (which keep the DDC stable during deformation). The image-derived forces are based on edges. So, it is necessary to initialize the DDC by drawing an approximate outline of the object.

In our approach, an operator first identifies and then crops out the vessel of interest in the given image. The operator then draws an approximate outline of the inner arterial wall in the form of a polygon with four to six vertices. The DDC is then deformed towards the inner (lumen/wall) boundary, with additional points automatically introduced to maintain a fixed spacing (patching) between points. In case of unsuccessful segmentation (e.g., if part of the contour undershoots an edge due to overdamping), individual points on the DDC can be manipulated, and the DDC is deformed again. Once the algorithm successfully finds the inner boundary of the arterial wall, this inner contour is saved and then inflated by approximately $626 \mu\text{m}$ (i.e., two pixels at the standard 16-cm FOV, and roughly equal to the wall thickness of a normal carotid) to create a ‘second contour’ as the initial approximation for the outer arterial wall boundary. This second contour is then automatically

deformed and saved to fit the outer arterial wall boundary in the same manner as described for the inner contour.

Object Recognition

In evaluation approaches, the overall vascular volume delineated by segmentation may not match with segmentation truth i.e. some areas of a vessel may be missed regions in delineation. If it is a crucial landmark area, such as a location of lesions, vascularization then missing or overestimating could affect important clinical-decision making for the location of vital regions such as vulnerable plaque fibrous cap. It highlights the algorithm's recognition performance.

Prerequisites of object recognition: Plaque as true surrogate needs reliable information for assessing accuracy of segmentation. It needs *a priori* information related to the object (recognition) based on the following strategy:

1. Compile a list of features/landmarks that are vital for $\langle X, Y, Z \rangle$ through help from a set of experts (radiologists, surgeons, cardiovascular-anatomists).
2. Each expert assigns a score to each feature to indicate its level of importance in $\langle X, Y, Z \rangle$.
3. Compute an average of the scores. Normalize these to the range $[0, 1]$. It generates a feature vector F whose components have values in $[0, 1]$.
4. Experts locate and delineate the critical plaque area of these features in scenes in T repeatedly.
5. Use the mean location and spread information and the mean vector F to generate a scene C_{tr} , (for each scene $C \in T$) which is a composite of the Gaussian weighted scores for all features in the set. In this composite scene $C_{tr} = (C, f_{tr})$, a high value $f_{tr}(c)$ for a voxel $c \in C$ indicates that c is both close to the mean location for a particular feature.

It generates a scene e_{tr} for each feature i in F or make C_{tr} , a vectorial scene. Alternatively, these individual scenes e_{tr} may be combined into a composite scene C_{tr} , as indicated above by taking an average or a fuzzy union. In any case, let S_{tr} , denote the set of resulting scenes containing information about truth in object recognition. Object recognition measurements on segmented contours: Other approach may be using the inner and outer contours (C_{in} and C_{out}), to compute six measures: 1) arterial wall area (A_w); 2) average radius of C_{in} (R_{in}); 3) average radius of C_{out} (R_{out}); 4) signal difference to noise ratio (SDNR) at the inner wall-blood interface ($SDNR_{in}$); 5) SDNR at the tissue-outer wall interface ($SDNR_{out}$); and 6) SNR within the wall.

Using this approach, wall area was calculated by subtracting the area enclosed by C_{in} from the area enclosed by C_{out} . Since the computed wall areas are dependent on both C_{in} and C_{out} , R_{in} and R_{out} were calculated to characterize the effects of resolution and noise on these contours individually.¹² R_{in} was calculated by finding the average distance between C_{in} and its centroid. R_{out} was calculated similarly from C_{out} .

For ‘edge detection’ algorithm, a particularly convenient and appropriate measure is the SDNR difference at the inner wall-blood interface ($SDNR_{in}$) and the tissue-outer wall interface ($SDNR_{out}$) to detect the edge between the regions. SDNR served as objective measure of quality for interfaces. It is calculated by taking the ratio of the signal difference at the interface of interest and the standard deviation (SD) of pixel values with in an area of no signal. Each inner-outer wall boundary contour pair (C_{in} and C_{out}) from a given image generated two additional contours automatically: a deflated inner boundary contour (C_{def}) was created by moving the nodes of the inner boundary contour 626 μm inward in a direction normal to C_{in} while an inflated outer contour (C_{inf}) was created by moving the nodes of C_{out} 626 μm outward in a direction normal to C_{out} . It calculates $SDNR_{in}$ by subtracting the mean pixel value of the wall region (bounded by C_{in} and C_{out}) from the mean pixel value of the blood boundary

region (bounded by C_{def} and C_{in}) and dividing by the SD of pixel values in the blood-core region (enclosed by C_{def}). In the same way, $SDNR_{out}$ is calculated by subtraction of the mean pixel value of the tissue-boundary region (bounded by C_{inf} and C_{out}) from the mean pixel value in the wall region (bounded by C_{in} and C_{out}) and dividing it by the SD of pixel values in the blood-core region. Mean pixel value of the wall region (bounded by C_{in} and C_{out}) divided by the SD of pixel values in the blood-core region gives SNR. So, both $SDNR_{in}$ and $SDNR_{out}$ are measures of “interface quality” associated with the C_{in} and C_{out} contours.

3D reconstruction and 3D rendering analysis

Three-dimensional analysis of stacked gray scale images or of stacked binary image was performed on computer as geometrical transformations (rotation, translation and zooming) by use of the “reslicing” and “projective imaging” tools of the NIH-Image 1.63 software.¹² Volumetric analysis was be done after 3-D reconstruction in rotating frame using Vision 2.5 software as described with example in the following results. 3D reconstruction was done by use of contour image series of the specimen surfaces and of the internal structures display. Marching cube algorithms generated three-dimensional models based on feature vectors and cluster partitioning for geometrical transformation, projection, hidden-part removal and shading. These models can be viewed from all angles and can be animated for enhanced 3D effect using the “Vascular Display” module of the image Vision 2.5 software. Commonly available alternative methods of rendering are z-buffer technique, ray-casting, ‘surface approximation’ and ‘voxel projection’ in vascular 3D rendering based on distinct blocks of different translucencies (opacity) of each binary scene (vascular regions at plaque interface) at various angles. In other words, different density of each voxel shows distinct opacity and color.

Imaging and Postprocessing

Image Acquisition for Carotid Artery Bifurcation

MRI images (n=14) were used for segmentation and registration. These MRI images were earlier acquired as part of a pilot study using 1.5 T GE Signa Lx Horizon attached Cardiac Imaging system at Methodist Hospital, Houston with ECG gating and appropriate parameters (Table 1) to get images with the same or nearly-same phase of cardiac cycle.¹⁰

Multicontrast Protocol

With a multicontrast protocol using T1-, proton density-, and T2-weighted images generated actual area of carotid artery with different tissue features due to their different Larmor frequencies of plaque constituents resulting in specific T1 and T2 values and signal intensities.^{12, 13}

T1 Parametric Contrast Method

Two 3D image analysis algorithms, one a nearest-neighbor (ANN) tissue segmentation algorithm, the other a 'surface modeling' algorithm, were applied to serial MR images.¹⁴ The algorithms operate on different principles to determine tissue volume: the nearest-neighbor approach used manually identified 'tag' points to assist in classifying tissue types while 'boundary' and 'volumes' are calculated automatically. The

surface-modeling algorithm relied on manual segmentation while volume determination was automated. Volumes of contrast enhancement and rates of volumetric change were determined by both algorithms. The tissue segmentation algorithm was used to create 3D maps.¹⁴

T2 Parametric Imaging for Segmentation and Quantification of Plaque Components

T2 parametric segmentation was based on their TE and TR values as earlier described elsewhere.¹⁵

Supervised Semi-automated Parametric Color-coded Segmentation Method

Color-coding segmentation by using k-nearest neighbor algorithm (k-NN) was utilized to create a stack of color-coded segmented image slices. It discards seed points. Connectivity algorithm classifies the color coded features. The method was based on color-coded pixel intensity probability distribution.¹⁶ Similarly, voxel-coding probability provides voxel-by-voxel parameters for automated structure parameterization. A supervised classifier was used to derive binary map. In each 2D slice a fast algorithm propagates a distance field from image exterior to interior. Local maxima distances were identified. The second shortest voxel paths to exterior were also identified. A third distance field is traversed to establish object connectivity between slices, and resulting voxel set is uniformly re-parameterized and triangulated as described in detail elsewhere.¹⁷

Table 1 Scan imaging parameters of the different pulse sequences for image acquisition with different T1/T2/proton density (PD) weighting for carotid artery bifurcation.

| Plane | Slices | Pulse sequence | PSD | Flip Angle | TR/TE | Gated BW | Thick/Sp | FOV | Matrix | NEX weight |
|----------|--------|----------------|--------|------------|----------|----------|----------|-------|--------|------------|
| Sagittal | 11 | FSE,ETL=12 | - | 90 | 2000/26 | - | 64 | 4/4 | 24x24 | 1 PD W |
| 2D TOF | 50 | GRE,ETL=12 | 2DTOF | 60 | 24/5 | - | 64 | 1.5/0 | 16x12 | 1 T1 W |
| Axial | 6 | FSE,ETL=8 | - | 90 | 2200/32 | 2RR | 64 | 3/0 | 13x13 | 2 PD W |
| Axial | 5 | FSE,ETL=3 | - | 90 | 550/16 | - | 32 | 3/0 | 13x13 | 2 T1 W |
| Axial | 6 | FSE,ETL=18 | FSE-XL | 90 | 2500/108 | 3RR | 62 | 3/0 | 13x13 | 3 T2 W |

3D Reconstruction Display

Volume rendering was done by using Volume J a java image processing program for DICOM multi-slice stacked images. For surface rendering, VISION 5.4 and VTK software generated 3D graphic view of vascular frame.¹⁸

Plaque Volume Measurement

It may be calculated from the outer wall radius (R) and inner wall radius (r) and length of plaque rich segment as:

$$V_{(\text{maximum})} - V_{(\text{minimum})} = L(2R+r) B/6 \quad (9)$$

where B is small plaque-rich region on MR image of the plaque. The difference in outer and inner wall volumes comes out as plaque volume as validated elsewhere¹⁹ and shown in Figure 10.

Results

The 3D TOF FSE images showed distinct quantifiable wall boundaries, however, different flow rates appeared visibly to artifact these image signal intensities (Figure 1). Wall thickness and atheroma size were main distinct features to assess plaque stenosis and vulnerability.

Multislice comparison showed good agreement between segmentation truth and postsegmented delineated wall measurements of inner and outer wall perimeters, lumen size and plaque curves at the bifurcation landmark on in vivo MRI images (Figures 2-4). Interestingly, at different levels of carotid vessel after supervised multiparametric color-coded feature maps of the lumen size and wall thickness gave an estimate of extent for % stenosis and plaque tissue proton density with distinct color (Figure 5). For true estimate of dimensions, intact plaque and its histology section with plaque features are shown (Figure 6).

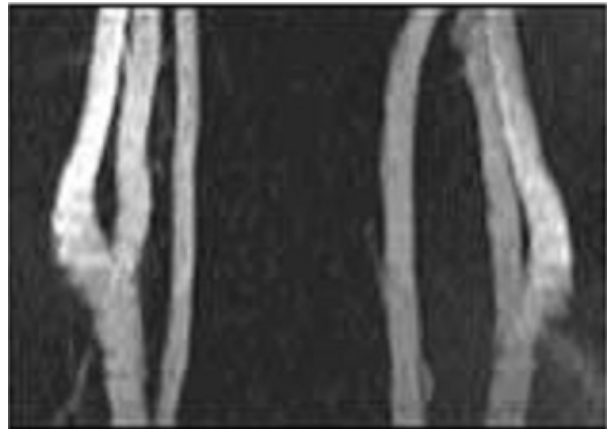


Figure 1 3D TOF FSE images of carotid artery at the level of bifurcation show distinct plaque sites.

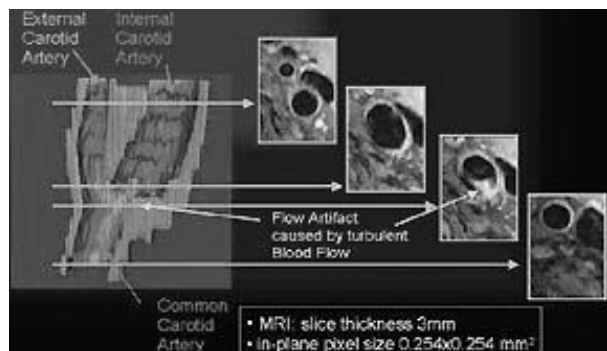


Figure 2 An in vivo postsegmented carotid artery plaque shows the distinct wall thickness and delineated wall boundaries representing different wall thickness in different slices.

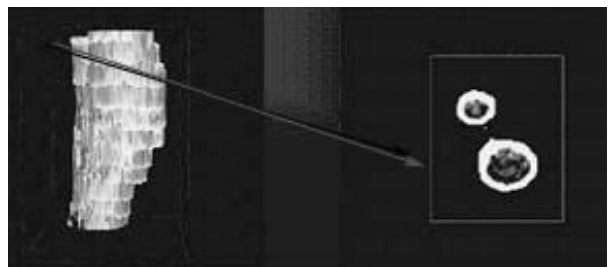


Figure 3 The method of 3D multislice stereographic display at different levels (left) and wall delineation by SNAKES algorithm demonstrates the measurement of outer and inner wall radii (right).

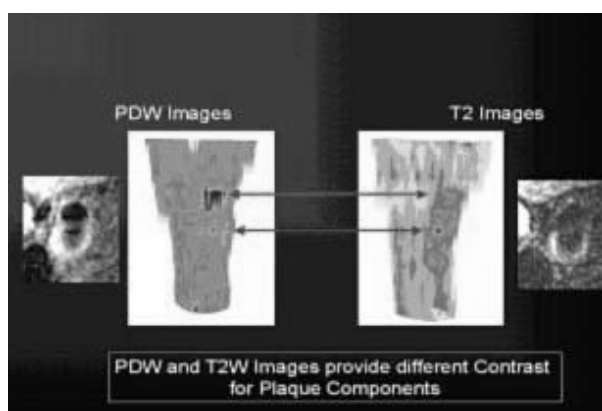


Figure 4 Supervised multiparametric color-coded feature maps show lumen size and wall thickness (left panel). Contours with different signal intensities of different plaque constituents (right panel). Notice the plaque visibility on in vivo images.

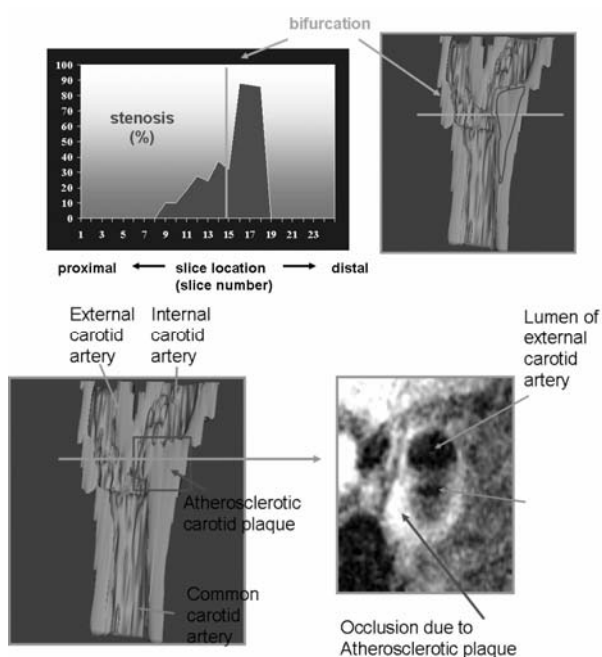


Figure 5 Semiautomated delineation is shown on multiparametric color-coded feature map to demonstrate the measurement of % stenosis (top panel) and lumen size (bottom panel).

T1 parametric contrast: T1 values of images provided less information than T2 values or proton density images. Due to dependence of T1 and T2 relaxation times upon magnetic field, it might not allow same MRI criteria. It needed appropriate TE and TR choice for in vivo

microimaging application using 1.5 T MRI clinical imager. However, wall measurement in postsegmented carotid arteries was better due to sharp edges (Figure 7) while plaque features were poorly measurable.

T2 parametric contrast: Specifically, spin-spin relaxation time T2 of image micro-dissected necrotic core at different sets of TE settings, overcome the problem of observed darker T2 images than actual low signal of plaque components e.g. fibrocellular and thrombus contents. On other hand, the wall measurement was not as good as measured by T1 parametric segmentation (Figure 8).

Multiparametric contrast: Combined T1/T2/proton density multiparametric approach allowed interactive segmentation by color cluster statistics (as 3D histograms) and tracking stereo display of different tissue constituents (Figure 9).¹⁵

3D Reconstruction: 3D reconstruction of staked DICOM images showed as contiguous display. The plaque in situ 3D features were distinct and plaque volume measurement was based on using curvature and outer and inner radii (Figure 10).

Volume rendering and 3D display: NIH Image J interfaced with Volume J was used for 3D graphic display and staked cross-sectional 3D display was obtained by VTK software. The minimum intensity projection (MIP) stacked slices demonstrated the calcification on transverse sites while 3D surface rendering demonstrated features in longitudinal sites along the wall (Figure 11).

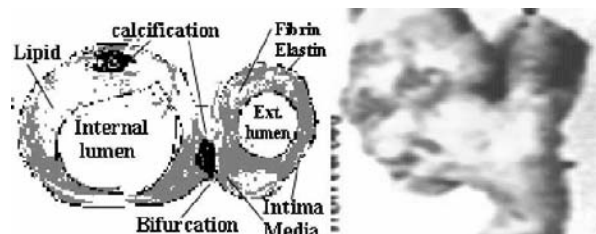


Figure 6 A comparison of plaque histology (left panel) and endarterectomy (right panel) shows true wall thickness and plaque features as surrogate markers for MRI segmentation.

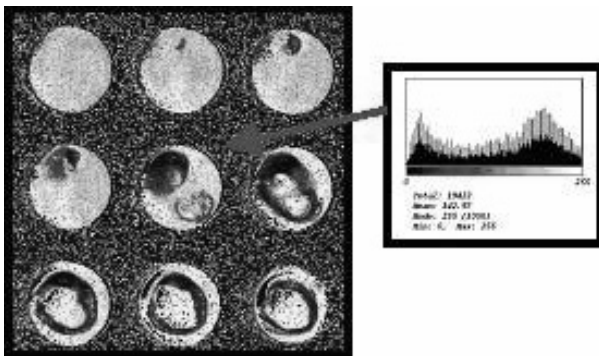


Figure 7 T1 parametric segmentation is shown to highlight wall thickness at various segments as contiguous postsegmented images of carotid endarterectomy sample.

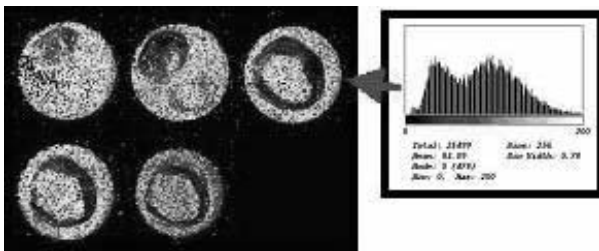


Figure 8 T2 parametric segmentation is shown to highlight wall thickness at various segments as contiguous postsegmented images of carotid endarterectomy sample.

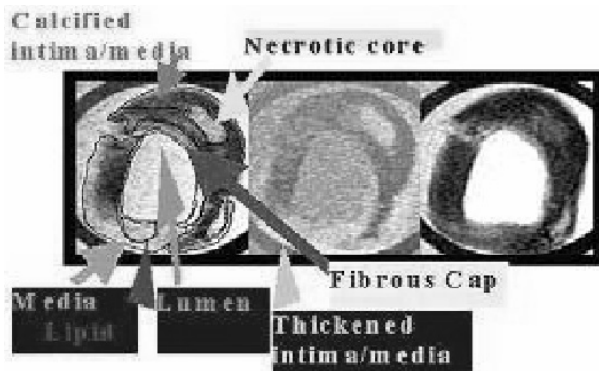


Figure 9 Multicontrast ex vivo MR images of a carotid endarterectomy sample shows distinct features of plaque on T1-weighted (left); proton density-weighted (in center); and T2-weighted (right) images. Plaque delineated features are shown with arrows.

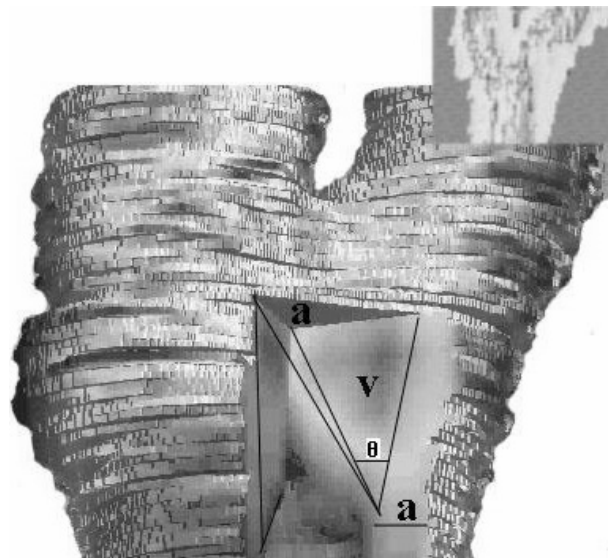


Figure 10 A set of postsegmented stacked carotid endarterectomy images shows reconstructed image 3D display. The display demonstrated the plaque size V and wall area 'a' features at various angles θ . The insert on top shows the plaque dimension in one cross-section.

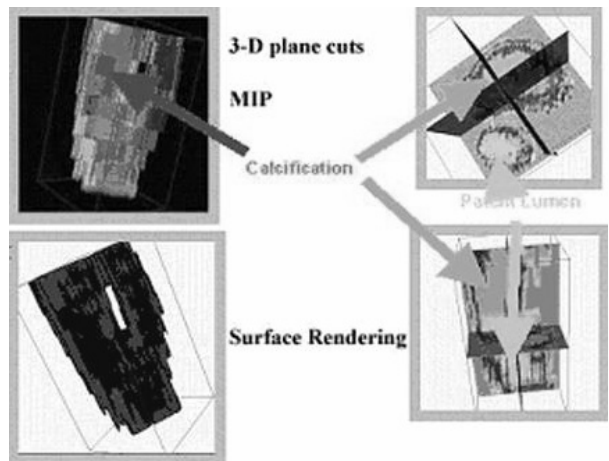


Figure 11 Continuous display of endarterectomy sample shows the 3D reconstructed MIP images (top left); 3D plane cut to show calcification in transverse plane (top right); surface rendering in 3D box (bottom left); and 3D plane cut to show calcification in longitudinal plane (bottom right).

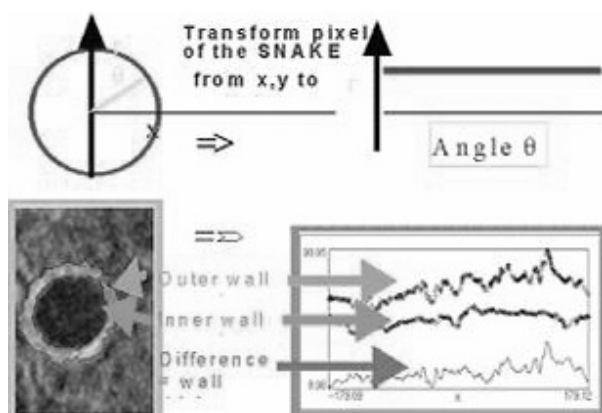


Figure 12 Deformable model and SNAKES parametric method shows the contours on outer and inner walls to measure wall thickness (bottom right).

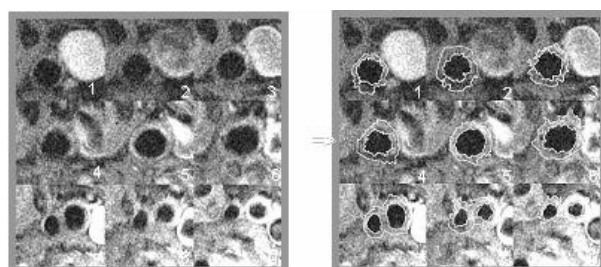


Figure 13 A semi-automated delineation method shows the outer and inner boundaries of carotid walls on serial slices of an endarterectomy sample (right). For comparison, different serial image slices are shown before delineation (left).

Deformable models and SNAKES for wall thickness segmentation: Deformable parametric models of contours of outer and inner walls generated automated wall thickness curves at different levels of carotid artery (Figure 12). The SNAKES as contours were pixel transformations at different angle. The semi-automated method of delineation in contiguous image slices may be summed up to measure total plaque burden (Figure 13). The measurement accuracy of outer and inner wall is demonstrated in in vivo MRI image (Figure 14).

Evaluation of segmentation: Deformable models extracted out the carotid plaque boundaries and wall thickness from MRI images and generated parametric curve and parametric surface by object delineation (plaque and lumen size) and

bifurcation landmark as surrogate marker. Object recognition was accomplished by distinct T1, T2 and proton density signal intensities of plaque features and clear edges of carotid vessel wall.

Color-coded feature maps: Non-parametric trained data sets of feature maps shown measurable lumen size and wall thickness at various transverse sections. These could be used as indicators of tissue composition (Figure 14).

Plaque Voluming: Outer and inner radii and size of plaque rich segment, volume of plaque from in vivo MR images was measured. However, other method of plaque volumetry used summing up of all plaques areas in every slice (Figure 10).

Discussion

Carotid artery atherosclerosis imaging is investigated as important clinical-decision making modality for plaque vulnerability. 3D segmentation techniques are in developing stage but very promising in tissue classification using in vivo MRI methods. 2D/3D time-of-flight FSE or GRE methods are now available for fast vascular imaging. So, segmentation plays crucial role and as challenge due to its several trade-offs. Main emphasis was focused in recent years on dimensionality and quantification of carotid artery morphology features. However, success was limited but encouraging for parametric and non-parametric segmentation on one hand while 3D voluming and surface or volume rendering showed window for time-dependent dynamic angiography applications. Present time interest in plaque constituents and feature analysis at different levels of carotid bifurcation image slices was reported as good indicator of plaque instability and vulnerability.²⁰ Of specific mention, these images of carotid artery on multicontrast (using T1, T2 and proton density) protocol visualize better segmentation and contrast information on these three image sets. In previous report, T1/T2/proton density multiparametric approach allowed interactive segmentation by color cluster statistics

(as 3D histograms) and tracking stereo display of different tissue constituents.²¹ Carotid artery bifurcation is used as a landmark for overall vessel segmentation process.

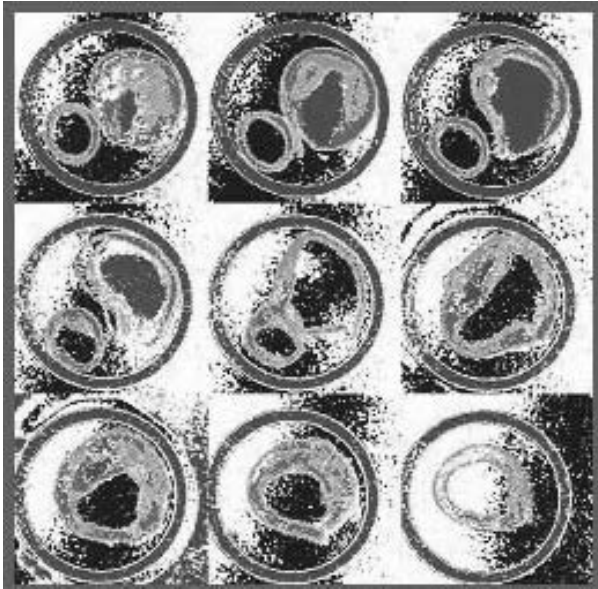


Figure 14 A set of transverse color-coded post-segmented feature maps of an atherosclerosis plaque at different levels show wall delineation and lumen size. It calculates the vascular wall composition as shown distinct colors of different features.

3D skeleton build-up is important approach as guide map for segmentation. From quantification point of view, center of vessel and *a priori* knowledge of carotid artery is important for segmentation tasks such as artery-vein separation, object extraction. Most of the time, image acquisition suffers from partial volume effects and intensity non-uniformities. From the quantitative point of view, several segmentation methods overcome these non-uniformities. Among them, of special importance are thresholding (shape-based histogram techniques, optimal thresholding either by non-parametric optimal or parametric optimal, Maximum Likelihood methods) and edge-based methods (border tracing, graph searching, dynamic programming, advanced border detection, Hough transforms). Other methods include region-based segmentation (region growing, region splitting and merging, connected component labeling) and

various classification methods, such as clustering algorithms (parallelepiped, minimum distance, K-means ISODATA, Fuzzy C-means), Bayes classifiers, k-NN, Adaptive fuzzy c-means with INU estimation, decision trees, ANN (Feed forward ANN, Kohonen ANN) and contextual classifiers.²²

In this study, the display of three-dimensional angiograms used *a priori* knowledge of quantitative shape features such as tangent and curvature of the centerline of vessels. These could be obtained in previous reports from a curve-like skeleton representation.²³ If connectivity and topology were preserved, and if geometrical constraints such as smoothness and centeredness were satisfied, it was possible to estimate length, orientation, curvature, and torsion (Figure 2). An efficient robust method for the identification of such shape components was developed. First, a suitable representation was obtained using a voxel-coding approach to yield connected and labeled unit-thick paths. The desired features were estimated from a smoothed version of the skeleton produced by a moving average filter.²⁴ Previously, most investigators reported standard fast spin-echo sequences for atherosclerotic plaque distinct MRI signals appearing as darker lipid rich core and lighter fibrocellular tissue by T2-weighted sequences.^{8,9} These factors were highlighted in this study showing further the need of T1-weighting using frequency selective sequences with very short TE for achieving good contrast between atheroma and fibrous tissue. In recent studies, monitoring of progression or regression of atherosclerotic lesions of carotid aorta and lumen stenosis or wall thickening in serial images and use of 2-D/3-D fast spin-echo proton density weighted images improved contrast-to-noise ratio and discriminated lumen, peri-adventitial fat and plaque. Common carotid intima-media thickness and atherosclerotic lipid-rich plaque characterization at carotid bifurcation served as unique indicators of generalized atherosclerosis. Other approach of enhancing in-plane resolution was based upon using short TE, T2 weighting MR imaging to define better plaque region by Morrisett et al.¹⁰ In that study, intravascular T2 weighted

imaging generated better MR contrast resolution. It served well by placing phased array coils closer to carotid artery wall using short TE for 'high spatial resolution' weighted images. The present report supports previous multicontrast approach of selection (T1/T2 and proton density weighted MRM) to acquire maximum signal-to-noise ratio (SNR) for better segmentation of plaque components in 1 mm thick MRM slice. Differentiation of plaque components by T2 contrast resolution at 9.4 T generates discriminated plaque structural components after segmentation to distinguish calcification, fibrous, collagen, elastin, hemorrhage, crystalline cholesterol, other lipids based upon different MR signal intensities due to their MR visible distinct proton species. Atheroma and fibrous cap in plaque images are generally considered to represent plaque instability and generate optimized contrast by selecting TE and TR values.¹⁰

Parametric imaging of segmentation and quantification of plaque components based on their TE and TR values could be accomplished with high degree of sensitivity and specificity on T1 parametric and T2 parametric segmentation. T1 parametric segmentation was better for vessel geometry and T2 parametric segmentation was better for classification. These values appear to provide information of noninvasive in vivo application of MRI criteria. Specifically, T2 values micro dissected the necrotic core at different sets of TE values to overcome the problem of observed darker T2 images than actual low signal of plaque thrombus and fibrous components. T1 weighted images provide less information than T2 weighted images or proton density weighted images. So, it needs appropriate TE and TR choice for in vivo microimaging application.

In supervised semiautomatic parametric segmentation generated color-coded feature maps for each plaque features that measured the composition of plaque. Interestingly, stacked image slices and the inclusion of T1 based images, as a third input, produced significant improvement in the delineation and curvatures of carotid vessel wall and it supports earlier reports.^{25,26} Volumetric

segmentation techniques visualize 3D to 2D projections such as object-based approach to reconstruct the artery but less known and possible future hope. However, these help to calculate the plaque volume and lumen quantification directly from MRI image by iterative dilatation approach by starting distal artery end traveling in proximal direction along the center of vessels, determining the lumen boundaries.¹⁸

3D reconstruction and surface and volume rendering techniques promise for cross-sectional multislice axial, coronal and sagittal comparisons and a future hope of 3D registration of multi-session studies for drug or therapy monitoring.^{12,20,21,27} The study has limitations due to its preliminary evidence to demonstrate the possibilities of less known robust segmentation power of different algorithms to be applied in clinical studies. Segmented images, however, may evaluate wall thickness, lumen size, plaque volumes, diagnosis, location of pathology, vascular anatomical structure, treatment planning, partial volume correction of vascular dynamic imaging data, and computer integrated endarterectomy.

Conclusion

Segmentation algorithms of 3D segmentation based on object delineation and object recognition of atherosclerosis vascular wall and plaque features; surrogate markers; validation with SNAKE algorithm provide evaluation of carotid artery atherosclerosis disease burden. It may be applied to in vivo MRI images of carotid artery vessels to estimate carotid artery atherosclerosis plaque burden and its feature identification. Segmented images can be used in femoral and other major vessels to evaluate the risk of atherosclerosis.

Acknowledgements

First author acknowledges his training at Atherosclerosis division, Baylor College of Medicine, Houston, TX, and all MRI data

acquisition and data figures as part of a pilot study done with Joel Morrisett, Ph.D, William Insull, MD and Wesley Wick, MD, Ph.D. He also acknowledges the computer facility access for all data analysis to Dr JK Katz at Cardiology Division, Columbia University, New York, NY. Partly, the experimental data was presented at RSNA 2000, ISMRM 2000 and AHA 2000 meetings.

References

1. Naghavi M, Libby P, Falk E, et al. From vulnerable plaque to vulnerable patient: a call for new definitions and risk assessment strategies: Part I. *Circulation* 2003; 108(14):1764-1772.
2. Glagov S, Bassiouny HS, Masawa N, Sakaguchi, Giddens DP, Zarins CK. Cerebrovascular Disease: A Pathologist's View. In *Syndromes of Atherosclerosis: Correlation of Clinical Imaging and Pathology*, Ed. Fuster V., Futura Publishing Company Inc., Armonk, NY. 1996, pp 161-180.
3. Liang Q, Wendelhag I, Wikstrand J, Gustavsson T. A multiscale dynamic programming procedure for boundary detection in ultrasound carotid artery images. *IEEE Trans Med Imaging* 2000; 19(2):127-142.
4. Chao H, Kerwin WS, Hatsukami TS, Hwang JN, Yuan C. Dynamic contours: Detecting objects in image sequences using rulebased control in an active contour model. *IEEE Trans Biomed Eng* 2003; 50(6):705-710.
5. Makowski P, Sorensen TS, Therkildsen SV, Materka A, Stodkilde-Jorgensen H, Pedersen EM. Twophase active contour method for semiautomatic segmentation of the heart and blood vessels from MRI images for 3D visualization. *Comput Med Imaging Graph* 2002; 26(1):917.
6. Pizer SM, Eberly DH, Morse BS, Fritsch DS. Zoom invariant vision of figural shape: The mathematics of cores. *Computer Vision and Image Understanding*, 1998; 69:5571.
7. Wink O, Niessen W, Viergever M. Fast quantification of abdominal aortic aneurysms from cta volumes. In *Proc. Medical Image Computing and Computer-Assisted Intervention (MICCAI'98)*, Berlin, Springer. 1998, pp 138145.
8. Troussaint JF, LaMuraglia GM, Southern JF, Fuster V, Kantor HL. Magnetic Resonance Images: lipid, fibrous, calcified, hemorrhagic, and thrombotic components of human atherosclerosis in vivo. *Circulation* 1996; 94(5):932-938.
9. Shinner M, Fallon JT, Wehrli S. The diagnostic accuracy of ex vivo MRI for human atherosclerotic plaque characterization. *Arteriovascular Thromb Vasc Biol* 1999; 19:2756-2761.
10. Morrisett J, Vick W, Sharma R, Lawrie G, Readon M, Ezell E, Schwartz J, Hunter G, Gorenstein D. Discrimination of components in atherosclerotic plaques from human carotid endarterectomy specimens by magnetic resonance imaging ex vivo. *Magn Reson Imaging* 2003; 21:465-474.
11. Ladak HM, Milner JS, Steinman DA. Rapid three-dimensional segmentation of the carotid bifurcation from serial MR images. *J Biomech Eng* 2000; 122(1):969.
12. Vinitiski S, Gonzalez CF, Knobler R, Andrews D, Iwanaga T, Curtis M. Fast tissue segmentation based on a 4D feature map in characterization of intracranial lesions. *J Magn Reson Imaging* 1999; 9(6):768-776
13. Beltrame F, Fato M, Raposio E, Sobel I. Recent results in color compositing of threeparameter magnetic resonance scans as a preoperative aid to the management of upper limb sarcomas. *MAGMA* 1997; 5(4):289-298.
14. Ishimori Y, Kimura H, Uematsu H, Matsuda T, Itoh H. Dynamic T1 estimation of brain tumors using double echo dynamic MR imaging. *J Magn Reson Imaging* 2003; 18(1):113-120.
15. Helms G. T2 based segmentation of periventricular paragraph sign volumes of quantification of proton magnetic paragraph sign resonance spectra of multiple sclerosis lesions. *MAGMA* 2003; 16(1):101-106.
16. Yi D, Hayward V. Skeletonization of volumetric angiograms for display. *Comput Methods Biomech Biomed Engineering* 2002; 5(5):329-341.
17. Woods RP, Grafton ST, Watson JD, Sicotte NL, Mazziotta JC. Automated Image Registration: II. Intersubject validation of linear and nonlinear models. *J Computer Assisted Tomography* 1998; 22(1):153-165.
18. Ashburner J, Friston KJ. Nonlinear spatial normalization basis functions. *Human Brain Mapping*. 1999; 7(4):254-266.
19. Sharma R. A device for MR imaging of atherosclerosis plaque in carotid endarterectomy specimens ex vivo. *Mag Res Med Sci* 2002; 1(2):129-136.
20. Zhang S, Cai J, Luo Y, Han C, Polissar NL, Hatsukami TS, Yuan C. Measurement of carotid

- wall volume and maximum area with contrastenhanced 3D MR imaging: Initial observations. *Radiology* 2003 Jul; 228(1):2005.
21. Long Q, Ariff B, Zhao SZ, Thom SA, Hughes AD, Xu XY. Reproducibility study of 3D geometrical reconstruction of the human carotid bifurcation from magnetic resonance images. *Magn Reson Med* 2003 Apr; 49(4):665-674.
 22. Dawant BM, Zijdenbos AP. *Image Segmentation*. Chapter 2 in *Handbook of Medical Imaging Volume 2. Medical image processing and analysis*, Eds. Sonka M, Fitzpatrick JM, SPIE Press, Washington, USA. 2000, pp 711-28.
 23. Yuan C, Lin E, Millard J, Hwang JN. Closed contour edge detection of blood vessel lumen and outer wall boundaries in blackblood MR images. *Magn Reson Imaging*. 1999; 17(2):257-266.
 24. Goubergrits L, Affeld K, Fernandez Britto J, Falcon L. Geometry of the human common carotid artery. A vessel cast study of 86 specimens. *Pathol Res Pract* 2002; 198(8):543-551.
 25. Clarke SE, Hammond RR, Mitchell JR, Rutt BK. Quantitative assessment of carotid plaque composition using multicontrast MRI and registered histology. *Magn Reson Med* 2003 Dec; 50(6):1199-1208.
 26. Cai JM, Hatsukami TS, Ferguson MS, Small R, Polissar NL, Yuan C. Classification of human carotid atherosclerotic lesions with in vivo multicontrast magnetic resonance imaging. *Circulation* 2002; 106(11):1368-1373.
 27. Merickel MB, Carman CS, Brookeman JR, Mugler JP 3rd, Brown MF, Ayers CR. Identification and 3D quantification of atherosclerosis using magnetic resonance imaging. *Comput Biol Med* 1988; 18(2):89-102.